



HAL
open science

Polyelectrolyte multilayer films as backflushable nanofiltration membranes with tunable hydrophilicity and surface charge

Wenqian Shan, Patrice Bacchin, Pierre Aimar, Merlin Bruening L, Volodymyr Tarabara V

► **To cite this version:**

Wenqian Shan, Patrice Bacchin, Pierre Aimar, Merlin Bruening L, Volodymyr Tarabara V. Polyelectrolyte multilayer films as backflushable nanofiltration membranes with tunable hydrophilicity and surface charge. *Journal of Membrane Science*, 2010, 349 (1-2), pp.268 - 278. 10.1016/j.memsci.2009.11.059 . hal-00570691

HAL Id: hal-00570691

<https://hal.science/hal-00570691>

Submitted on 4 Feb 2022

HAL is a multi-disciplinary open access archive for the deposit and dissemination of scientific research documents, whether they are published or not. The documents may come from teaching and research institutions in France or abroad, or from public or private research centers.

L'archive ouverte pluridisciplinaire **HAL**, est destinée au dépôt et à la diffusion de documents scientifiques de niveau recherche, publiés ou non, émanant des établissements d'enseignement et de recherche français ou étrangers, des laboratoires publics ou privés.



Open Archive Toulouse Archive Ouverte (OATAO)

OATAO is an open access repository that collects the work of Toulouse researchers and makes it freely available over the web where possible.

This is an author-deposited version published in: <http://oatao.univ-toulouse.fr/>
Eprints ID: 4055

To link to this article: DOI:10.1016/j.memsci.2009.11.059
URL: <http://dx.doi.org/10.1016/j.memsci.2009.11.059>

To cite this version: Shan, Wenqian and Bacchin, Patrice and Aimar, Pierre and Bruening, Merlin L. and Tarabara, Volodymyr V. (2010) *Polyelectrolyte multilayer films as backflushable nanofiltration membranes with tunable hydrophilicity and surface charge*. Journal of Membrane Science, vol. 349 (n° 1-2). pp. 268 - 278. ISSN 0376-7388

Any correspondence concerning this service should be sent to the repository administrator: staff-oatao@inp-toulouse.fr

Polyelectrolyte multilayer films as backflushable nanofiltration membranes with tunable hydrophilicity and surface charge

Wenqian Shan^a, Patrice Bacchin^b, Pierre Aimar^b, Merlin L. Bruening^c, Volodymyr V. Tarabara^{a,*}

^a Department of Civil and Environmental Engineering, Michigan State University, A132 Engineering Research Complex, East Lansing, MI 48824, USA

^b Laboratoire de Génie Chimique, Université Paul Sabatier, 31062 Toulouse Cedex 9, France

^c Department of Chemistry, Michigan State University, East Lansing, MI 48824, USA

A B S T R A C T

A diverse set of supported polyelectrolyte multilayer (PEM) membranes with controllable surface charge, hydrophilicity, and permeability to water and salt was designed by choosing constituent polyelectrolytes and by adjusting conditions of their deposition. The membranes were characterized in terms of their water and MgSO₄ permeabilities and resistance to colloidal fouling. The commercial nanofiltration membrane (NF270) was used as a comparative basis. Highly hydrophilic and charged PEMs could be designed. For all membranes, MgSO₄ permeability coefficients of NF270 and all PEM membranes exhibited a power law dependence on concentration: $P_s \propto C^{-\tau}$, $0.19 < \tau < 0.83$. PEM membranes were highly selective and capable of nearly complete intrinsic rejection of MgSO₄ at sufficiently high fluxes. With the deposition of colloids onto the PEM surface, the separation properties of one type of polyelectrolyte membrane showed similar rejection and superior flux properties compared to NF270 membranes. We hypothesize that a PEM-colloid nanocomposite was formed as a result of colloidal fouling of these PEM films. The feasibility of regenerating the PEM membranes fouled by colloids was also demonstrated. In summary, the PEM-based approach to membrane preparation was shown to enable the design of membranes with the unique combination of desirable ion separation characteristics and regenerability of the separation layer.

Keywords:

Nanofiltration
Polyelectrolyte multilayer films
Colloidal fouling
Salt rejection
Regeneration
Backflushing

1. Introduction

Polyelectrolyte multilayer (PEM) films are prepared by alternately adsorbing oppositely charged polyelectrolytes onto supports using a layer-by-layer technique [1–3] and can serve as regenerable surface coatings with controllable physicochemical properties (e.g. charge, hydrophilicity, swellability, stiffness) that regulate adhesion to the surface [4–6]. Several groups used PEMs to render various surfaces resistant to adsorption of different proteins [6–15], mammalian cells [12,13,16–20], or bacteria [14,17,21,22]. Importantly, PEMs can also be designed to provide a selective barrier to aqueous ionic species [23]. When assembled on a surface [24–28] or within the inner pore structure [29] of a porous membrane support, PEMs can function as nanofiltration [24–28] or reverse osmosis [30] membranes to separate mono-, di-, and multivalent cations and anions [24–28,30–32] or neutral molecules [33–36]. For example, membranes composed of five bilayers of poly(styrene sulfonate)/poly(allylamine hydrochloride) (PSS/PAH) on porous

supports allow a high flux at regular nanofiltration pressures and exhibit 95% rejection of MgCl₂ along with a Na⁺/Mg²⁺ selectivity of 22 [37]. As another example, 4.5-bilayer PSS/poly(diallyldimethyl ammonium chloride) (PDADMAC) films on porous supports show Cl⁻/F⁻ and Br⁻/F⁻ selectivities larger than 3 along with solution fluxes that are 3-fold higher than those of commercial membranes [38].

The PEM approach to membrane design is highly versatile in that separation and antiadhesive properties of PEMs can be adjusted through the choice of the constituent polyelectrolytes, the number and sequence of polyelectrolyte layers in the film, and the deposition conditions (solution pH and ionic strength, e.g. [25]). A unique advantage of some PEM membranes is that when appropriately constructed, the film can be removed from the porous support via exposure to solutions with high pH values (10–12) or ionic strengths [39–41]. The film can then be regenerated through the layer-by-layer process. Thus, a PEM film assembled on a UF support can combine separation and antiadhesive properties with the ability to renew the surface (Fig. 1).

Nearly all studies on the separation properties of PEMs employed synthetic feed solutions with only one or two compounds in solution. The performance of PEM membranes challenged

* Corresponding author. Tel.: +1 517 432 1755; fax: +1 517 355 0250.
E-mail address: tarabara@msu.edu (V.V. Tarabara).

by suspensions of colloids (other than proteins) and regeneration of fouled PEMs have not been investigated. Very little is known about the effects of operational variables on PEM separation properties. In the only published study on the topic, Tieke and coworkers examined rejection with a very dense 60-bilayer poly(vinylamine)/poly(vinylsulfate) PEM membrane as a function of transmembrane pressure [30]. They observed pronounced concentration polarization effects, but a rigorous analysis was not possible because the study was conducted in a dead-end geometry. Importantly, while PEMs have been effective in simultaneously increasing protein retention and reducing protein adhesion [8], there have been no reports on the design of PEM membranes that combine resistance to colloidal fouling with desirable ion separation properties. This study aims at filling some of these knowledge gaps. Specific objectives of this work are:

- 1) to evaluate water and solute permeabilities of a diverse set of PEM membranes to understand the dependence of rejections on pressure and solute concentration;
- 2) to determine how the permeability and rejection of PEM membranes are affected by concentration polarization and colloidal fouling;
- 3) to assess PEM regeneration alternatives, including backflushing, for as-prepared PEMs and PEMs fouled by colloids.

2. Approach

Nanofiltration properties of PEM-coated membranes were compared with the corresponding properties of a commercial membrane, NF270. First, permeability to deionized water and MgSO_4 rejection were measured for all membranes in crossflow experiments. Solute transport to the membrane surface and transport across the membrane were modeled using a thin film model and Kedem-Katchalsky equations, respectively. Measured values of the permeate flux and the concentration of solute in the permeate were used to determine the MgSO_4 permeability coefficients of the membranes. By performing the crossflow experiments at a range of transmembrane pressure differentials, a range of concentration polarization conditions was tested, and the concentration dependence of MgSO_4 permeability coefficients was recorded for each membrane.

Second, the performance of membranes under conditions of colloidal fouling was evaluated in experiments on crossflow filtration of SiO_2 colloids suspended in an electrolyte solution. Based on (i) the measured values of permeate flux and Mg^{2+} concentration in the permeate and (ii) the previously determined MgSO_4 permeability coefficient as a function of concentration, the resistance to the permeate flow due to the deposited layer of colloids was computed for each membrane and used as a measure of the extent of colloidal fouling.

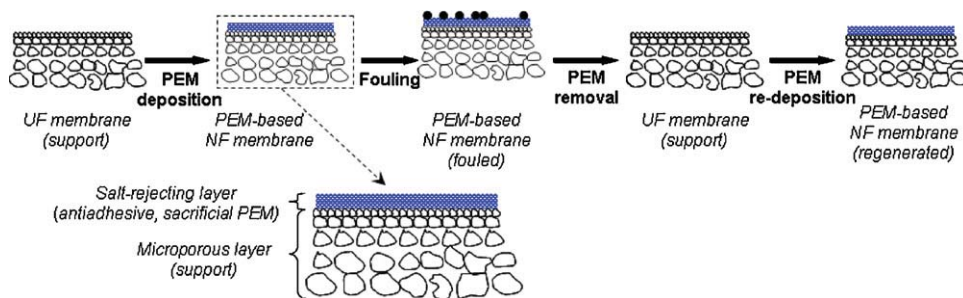


Fig. 1. Conceptualized drawing of the application and regeneration of a polyelectrolyte multilayer (PEM) nanofiltration membrane. The support thickness is not drawn to scale.

2.1. Determination of intrinsic rejection

To characterize the selectivity of membranes, MgSO_4 rejection was measured. The mass transfer coefficient, k , for MgSO_4 in the membrane cell channel was estimated from the Sherwood correlation ([42]):

$$Sh = \frac{kd_h}{D} = \left(3.66^3 + 1.61^3 Re \cdot Sc \cdot \frac{d_h}{L} \right)^{1/3}, \quad (1)$$

where Sh is the Sherwood number, L is the channel length, D is the diffusion coefficient of MgSO_4 in water ($8.5 \times 10^{-10} \text{ m}^2/\text{s}$ [43]), Re is the Reynolds number, Sc is the Schmidt number, and d_h is the hydraulic diameter of the channel. For the membrane cell used in this study, $d_h \approx 2h$, where h is the channel height. The value of $(Re \cdot Sc \cdot d_h/L)$ was in the (9020–10,300) range (see SD3), which was close to the upper bound of the applicability range ($0.1 < (Re \cdot Sc \cdot d_h/L) < 10,000$) of Eq. (1).

The thin film model was used to estimate the concentration of MgSO_4 at the membrane surface, C_m [44]:

$$\frac{C_m - C_p}{C_f - C_p} = \exp\left(\frac{J}{k}\right) \quad (2)$$

and to determine the intrinsic rejection, R_{in} , as a function of the permeate flux, J , for all permeate sampling times:

$$R_{in} = 1 - \frac{C_p}{C_m} = 1 - \frac{C_p}{C_p + (C_f - C_p) \cdot \exp(J/k)}, \quad (3)$$

where C_p , C_f and C_m are the concentrations of MgSO_4 in the permeate, in the bulk feed, and in the portion of the feed directly adjacent to the membrane, respectively. In this study, permeate flux and salt rejection were measured at different transmembrane pressure differentials, ΔP , and values of R_{in} were determined as a function of J using Eq. (3). These experiments were conducted using colloid-free MgSO_4 electrolyte as the feed.

2.2. Determination of solute permeability coefficient

The coupled transport of solute and solvent in a membrane is described by the Kedem-Katchalsky equations [45]:

$$J = L_p(\Delta P - \sigma \Delta \pi), \quad (4)$$

$$J_s = \omega \Delta \pi + (1 - \sigma) J \bar{C}, \quad (5)$$

where J and J_s are volume and solute fluxes across the membrane, respectively, L_p is the hydraulic permeability of the membrane, σ is the reflection coefficient, and ω is the solute permeability. Volume flux is given by $J = J_w \tilde{V}_w + J_s \tilde{V}_s$, where \tilde{V}_w and \tilde{V}_s are molar volumes of water and solute, respectively and J_w is the permeate water flux across the membrane. In Eq. (5), \bar{C} is the logarithmic mean of the

average concentration of solute within the membrane:

$$\bar{C} = (C_m - C_p) \cdot \ln^{-1} \left(\frac{C_m}{C_p} \right) \quad (6)$$

For large volume flows and high concentration gradients across the membrane, the changing concentration profile inside the membrane can be taken into account by recording Eq. (5) in the differential form. Noting that

$$J_s = J C_p \quad (7)$$

and substituting the expression for the local osmotic pressure differential

$$\Delta\pi = n\phi RT[C(x) - C(x + \Delta x)] \quad (8)$$

into Eq. (5), one obtains the Kedem-Katchalsky expression for the volume flux across a differential element of the membrane:

$$J C_p = -\bar{P} \frac{dC}{dx} + (1 - \sigma) J \bar{C}, \quad (9)$$

where $\bar{P} = n\phi RT\omega\Delta x$ is the local solute permeability coefficient, n is the total number of constituent ions in the salt ($n = 2$ for MgSO_4), \bar{C} now has the meaning of the logarithmic mean of the average concentration of solute within the differential element, and ϕ is the osmotic coefficient, which is generally a function of the solute concentration [46] and can be calculated using the Pitzer equation [47].

Note that the physical meaning of σ can be deduced from the Spiegler-Kedem relationship [48] that is obtained by integrating the differential form (Eq. (9)) of the Kedem-Katchalsky expression (Eq. (5)) across the membrane in the presumption of concentration-independent phenomenological coefficients σ and \bar{P} :

$$R_{in} = \frac{\sigma(1 - F)}{1 - \sigma F}, \quad (10)$$

$$F = \exp \left(-\frac{J(1 - \sigma)}{P_s} \right), \quad (11)$$

where P_s is the solute permeability coefficient ($P_s = n\phi RT\omega = \bar{P}/\Delta x$). It follows from Eqs. (10) and (11) that the reflection coefficient, σ , represents the limiting value of the intrinsic rejection achieved at $J \rightarrow \infty$.

Experimental evidence indicates that P_s is generally concentration-dependent (e.g. [49–52]). Accordingly, in this study we used the Kedem-Kachalsky Eq. (5) to determine the MgSO_4 permeability coefficient as a function of concentration, $P_s = P_s(C)$. To compute $P_s = P_s(C)$, Eq. (5) was used in its modified form:

$$J_s = P_s(C_m - C_p) + (1 - \sigma) J \bar{C}, \quad (12)$$

In deriving Eq. (12) the following expressions for the solute permeability and osmotic pressure differential were used: $\omega = P_s/n\phi RT$ and $\Delta\pi = n\phi RT(C_m - C_p)$. By incorporating Eqs. (6) and (7), Eq. (12) can be rewritten as:

$$J C_p = P_s(C_m - C_p) + J(1 - \sigma) \frac{C_m - C_p}{\ln(C_m/C_p)}. \quad (13)$$

The reflection coefficient σ was presumed to be concentration independent and its value was approximated by the maximum value of intrinsic rejection, R_{in}^{\max} . The error introduced into the computation of $P_s = P_s(C)$ by presuming the reflection coefficient to be concentration independent was at most 17% (see SD, section SD1). This value was obtained by measuring rejection at the highest experimental permeate flux in each conditioning experiment and calculating R_{in}^{\max} from Eq. (3). With σ available, the only unknown in Eq. (13) is P_s . By measuring J and C_p in an experiment on the filtration of colloid-free electrolyte (i.e. membrane conditioning stage of experiments; see Section 3.5) and computing C_m using Eq. (2)

and the Sherwood correlation (1), we applied Eq. (13) to determine P_s for the given C_m . By performing the above procedure at a series of different transmembrane pressure differentials ΔP (and, correspondingly, different permeate fluxes, J), the dependence $P_s = P_s(C)$ was determined for a wide concentration range for each membrane.

2.3. Quantifying concentration polarization and resistance of colloidal cake in colloidal fouling experiments

Under conditions of colloidal fouling, concentration polarization is enhanced due to the formation of a colloidal cake that hinders back diffusion of rejected salt [53,54]. With mass transfer correlations such as Eq. (1) available only for well-defined geometries and with the value of the hindered diffusion coefficient in the cake not known, thin film theory (Eq. (2)) can no longer be used to determine C_m . To overcome this difficulty, we fitted the experimental $P_s(C_m)$ data obtained in experiments on the filtration of colloid-free electrolyte solution (see SD, Fig. S2) to determine an analytical $P_s(C_m)$ expression. Then, Eq. (13) was used to determine the value of C_m for each sampling time in experiments on colloidal fouling (σ was assumed to be R_{in}^{\max} as mentioned above). Dividing C_m by the concentration of MgSO_4 in the feed, C_f , gives the concentration polarization factor, C_m/C_f , which can be determined at different times during the colloidal filtration experiment.

The hydraulic resistance exerted by the colloidal deposit, R_d , was computed using the following equation for the permeate flux:

$$J = \frac{\Delta P - \sigma \Delta\pi_m}{\mu(R_m + R_d)}, \quad (15)$$

where $\Delta P = P_b - P_p$ is the pressure differential between the bulk feed and the permeate, $\Delta\pi = \pi_m - \pi_p$ is the transmembrane osmotic pressure differential, R_m is the hydraulic resistance of the membrane, and μ is the water viscosity.

3. Experimental

3.1. Bench-scale crossflow filtration system

The detailed description of the crossflow filtration system is given in SD2. Briefly, a positive displacement pump was used to deliver the feed water to the high pressure membrane filtration cell. A pulsation dampener was installed immediately downstream from the pump outlet, and a back pressure regulator was used to maintain the transmembrane pressure differential at a constant value. Two in-line digital flowmeters were used to record the retentate and permeate fluxes every 30 s. Both permeate and retentate flows were directed back into the feed tank. In all colloidal fouling experiments, the retentate flow rate was maintained at (1.04 ± 0.07) L/min, which corresponds to a crossflow velocity of ca. 0.1 m/s and a Reynolds number of ca. 353 ± 24 . The temperature of the feed water was maintained at (20.0 ± 0.5) °C using a programmable circulating chiller.

3.2. Reagents and colloids

All reagents were of ACS analytical grade or higher purity and were used without further purification. Ultrapure water was supplied by a commercial RO/DI system (LabFive, USFilter Corp., Hazel Park, MI) equipped with a terminal 0.2 μm capsule microfilter (PolyCap, Whatman Plc., Sanford, ME). The resistivity of the water was greater than 16 $\text{M}\Omega \text{ cm}$.

Silica colloids (SnowTex-ZL, Nissan Chemical America Corp., Houston, TX) were received in the form of a concentrated suspension. Dynamic light scattering (BI-MAS particle sizing module, ZetaPALS, Brookhaven Instrument Corp., Holtsville, NY) was used to measure the particle size distribution in SiO_2 suspensions. Samples

Table 1

Ionic strength (I_c) and pH of the PEM solutions used to prepare PEM membranes. The adsorption time for each layer is listed in parentheses.

	[PSS/PDADMAC] ₄	[PSS/PAH] ₄	[PSS/PAH] _{4.5} ^a	[PSS/PAH] ₂ + [PAA]	[PSS/PAH] ₂ + [PAA/PAH] _{1.5} ^b
1st layer/ I_c /pH (adsorption time ^c)	PSS/0.5/6.4 ^d (3 min)	PSS/0.5/2.1 (2 min)	PSS/0.5/2.1 (2 min)	PSS/0.5/2.1 (2 min)	PSS/0.5/2.1 (2 min)
2nd layer/ I_c /pH (adsorption time ^c)	PDADMAC/0.5/4.6 ^d (3 min)	PAH/0.5/2.3 (5 min)	PAH/0.5/2.3 (5 min)	PAH/0.5/3.5 (5 min)	PAH/0.5/2.3 (5 min)
Terminating layer ^e / I_c /pH (adsorption time ^f)	PDADMAC/0.5/4.6 ^d (3 min)	PAH/2.5/2.3 (5 min)	PSS/2.5/2.1 (2 min)	PAA/2.5/4.5 (5 min)	PAA/2.5/4.5 ^c (5 min)

^a The subscript of 4.5 means that one single layer of PSS was deposited on top of the four [PSS/PAH] bilayers.

^b The pH of the PAH solution used in depositing the [PAA/PAH]_{1.5} was 3.5. The subscript of 1.5 means that one additional layer of PAA was deposited on top of one bilayer of [PAA/PAH].

^c The ionic strength of the solution used for depositing the first PAA layer in [PAA/PAH]_{1.5} was 0.5 mol/L.

^d The pH was that of the as-prepared PEM solution and was not adjusted.

^e The ionic strength of the solution during the deposition of the terminating layer was increased to 2.5 mol/L [26,37] except when PDADMAC was the terminating layer, because PDADMAC films dissociate at high ionic strength [41].

^f For strong polyelectrolytes, 3 min (for PDADMAC) or 2 min (for PSS) adsorption time was sufficient, while for weak polyelectrolytes such as PAH and PAA, a 5 min adsorption time was used.

were diluted with 0.1 mM MgSO₄ to reach the recommended count rate. The ζ -potential of particles was measured by a zeta potential analyzer (ZetaPALS, Brookhaven Instrument Corp., Holtsville, NY). The pH of the SiO₂ suspension in 0.1 mM MgSO₄ was in the 6.1–6.6 range. SiO₂ colloids were (140 ± 1) nm in diameter with a ζ -potential of (−30 ± 5) mV.

Mg²⁺ concentrations were determined using flame atomic absorption (AA) spectroscopy (Perkin-Elmer 1100, Waltham, MA). A stock solution of lanthanum chloride (Fisher Scientific) was added to all samples and standards to achieve a LaCl₃ concentration of 0.1% by weight. The calibration range for Mg²⁺ concentration was (0.1–0.6) mg/L.

3.3. Membranes

3.3.1. Preparation of polyelectrolyte multilayer membranes

A polyethersulfone (PES) membrane (Pall Corp., East Hills, NY) with a MWCO of 50 kDa served as the support for PEM films. The permeability of this UF membrane is considerably higher than that of the PEMs, but its surface porosity is sufficiently low to allow complete coverage of the support (i.e. complete bridging of the support's surface pores by the polyelectrolyte molecules) by PEMs with only a few adsorbed bilayers [27,55]. Prior to the PEM deposition, the support membranes were soaked first in 0.1 M NaOH for 3 h and then in deionized water for 24 h at 4 °C with water exchanged after the first 12 h of storage, as recommended by the manufacturer. Anionic and cationic polymers were alternately adsorbed on the UF substrate by immersing the substrate in the corresponding polyelectrolyte solutions with a 1 min water rinse after the deposition of each layer. Table 1 specifies the conditions for deposition of each layer for all of the polyelectrolyte membranes in this study.

Poly(diallyldimethyl ammonium chloride) (M_w = 100,000–200,000), poly(allylamine hydrochloride) (M_w = 70,000), and poly(styrene sulfonate) (M_w = 70,000) were purchased from Aldrich, and poly(acrylic acid) (M_w = 90,000, 25% aqueous solution) was obtained from Polysciences. The polyelectrolyte solutions were prepared at a repeat unit concentration of 0.02 mol/L, and the pH and ionic strength of polyelectrolyte solutions were adjusted using 1 M HCl, 1 M NaOH and 1 M NaCl solutions. The ionic strength of the solution during the deposition of the terminating layer was increased to 2.5 mol/L [26,37] except when PDADMAC was the terminating layer, because PDADMAC films dissociate at high ionic strength [41]. The deposition was always initiated with PSS to ensure the attachment of the multilayer membrane to the PES support due to hydrophobic interactions between PSS and PES [27]. The additional [PAA]-containing layers of [PSS/PAH]₂ + [PAA/PAH]_{1.5} and [PSS/PAH]₂ + [PAA/PAH]_{1.5} were added to increase the hydrophilicity of these membranes.

3.3.2. NF270 membrane as the comparative basis

Coupons of commercial polyamide thin-film composite NF270 membrane (FilmTec, Dow Chemical Company, Midland, MI) were cut from the as-received membrane sheet and soaked in ultrapure water for 24 h at room temperature prior to being characterized and used for filtration.

3.4. Membrane characterization

Streaming potentials of membranes were measured using an electrokinetic analyzer (BI-EKA, Brookhaven Instrument Corp., Holtsville, NY). Before the test, membranes were soaked in deionized water for 24 h. The KCl (pH 4) electrolyte solution used in these measurements had an ionic strength of 0.4 mM, which was the same that of the 0.1 mM MgSO₄ solution used in the filtration experiments.

To examine the hydrophilicity of the membranes water contact angles were measured using a FTÅ 200 contact angle analyzer (First Ten Angstroms, Portsmouth, VA). A 5 μ L drop of ultrapure water was formed on the tip of a stainless steel syringe needle and placed onto the membrane surface by raising the membrane until a contact was made. An image of the drop was taken (see SD, Fig. S3) 2 s after the drop formed on the surface, and the left and the right contact angles were determined. At least three membrane coupons were tested with five images taken for each membrane.

Scanning electron microscope images were recorded using a Hitachi S-4700II field emission SEM operated in ultrahigh resolution mode. Samples were mounted on aluminum SEM specimen stubs and made conductive by sputtering pure osmium (NEOC-AN, Meiwa Shoji Co. Ltd, Japan) for 30 s at a current of 10 mA.

3.5. Experimental protocol for crossflow filtration

Each crossflow filtration experiment was carried out in the following stages:

• Stage 1. Membrane compaction

Ultrapure water was filtered through the membrane for 24 h to ensure that irreversible compaction would not contribute to the flux decline observed in the colloidal fouling experiment. The transmembrane pressure differentials during compaction of membranes were set to exceed the pressures used in the fouling tests (Table 2). The impact of the compaction of the UF support on the separation properties of the overlying PEM layer was evaluated in experiments with [PSS/PAH]_{4.5} as a representative PEM. The water permeability and salt rejection were similar for PEM membranes deposited on compacted and non-compacted PES supports. In view of this result, the PEM membranes used in all the colloidal experiments in this study were prepared by depositing

Table 2
Transmembrane pressures and resulting permeate fluxes during SiO₂ filtration by PEM membranes. Also indicated are transmembrane pressures used to compact membranes prior to filtration tests.

Membrane	Transmembrane pressure, ΔP (psi)	Transmembrane pressure, ΔP (psi)	Initial permeate flux, $J \times 10^{-5}$ (m/s)	Initial specific permeate flux, $J/\Delta P \times 10^{-11}$ (m)/(s Pa)
	During compaction	During colloidal fouling tests		
[PSS/PDADMAC] ₄	40	11	2.8	36.3
[PSS/PAH] ₄	250	215	2.7	1.9
[PSS/PAH] _{4.5}	200	110	3.0	4.0
[PSS/PAH] ₂ + [PAA]	120	52	3.1	8.8
[PSS/PAH] ₂ + [PAA/PAH] _{1.5}	200	110	2.8	3.7
NF 270	220	122	2.8	3.3

the polyelectrolytes onto uncompact UF membranes. Subsequently, the PEM-coated membrane was compacted as described above.

• **Stage 2. Measurement of membrane hydraulic resistance**

After compaction, pure water permeate flux was recorded at several transmembrane pressure differentials: 80 psi (0.55 MPa), 120 psi (0.83 MPa), 160 psi (1.10 MPa) and 200 psi (1.38 MPa) for all membranes except [PSS/PDADMAC]₄. For [PSS/PDADMAC]₄, a sequence of lower pressures was used: 10 psi (0.07 MPa), 20 psi (0.14 MPa), 30 psi (0.21 MPa) and 40 psi (0.28 MPa). The hydraulic resistance, R_{m_0} , of the clean membrane to water was determined using linear least squares fitting of $J(\Delta P)$ to Eq. (16):

$$J = \frac{\Delta P}{\mu R_{m_0}} \quad (16)$$

• **Stage 3. Membrane conditioning and characterization**

5 mL of 0.4 M MgSO₄ was added to 20 L of ultrapure water in the feed tank to adjust the magnesium concentration to 0.1×10^{-3} M. The pH of the feed water was in the (6.1–6.6) range. Membranes were conditioned by filtering the electrolyte at the same pressure used in the 24 h water compaction stage until the permeate flux stabilized (ca. 20 h). When permeate flux getting stabilized after 20 h of conditioning, the transmembrane pressure was changed in step to achieve different permeate fluxes, J . During this process, permeate and feed water samples were periodically collected to determine values of the MgSO₄ rejection at different J . At the end of conditioning, the transmembrane pressure differential needed to achieve a permeate flux of $(2.8 \pm 0.2) \times 10^{-5}$ m/s was determined for subsequent use in the colloidal fouling experiment. Setting the initial permeate flux to the same value in all colloidal fouling tests ensured the same initial colloid deposition conditions in experiments with membranes with different values of water permeability, L_p .

• **Stage 4. Membrane fouling experiments**

15 g of SiO₂ ST-ZL stock solution was added into the 20 L of feed electrolyte to achieve a colloid loading of 300 mg/L. Crossflow filtration of the colloid-containing solution was then carried out for 20 h at the pressure determined in stage 3 to give an initial flux of $(2.8 \pm 0.2) \times 10^{-5}$ m/s. Small amounts of permeate and feed water were collected periodically to determine observed MgSO₄ rejection, R_{obs} . Each filtration experiment was conducted twice, and the flux profiles for the two membranes were reproducible with a maximum deviation of 11%.

• **Stage 5. PEM regeneration and backflushing test**

PEM removal and regeneration tests were performed with [PSS/PAH]₄ and [PSS/PAH]_{4.5} membranes only. To remove the PEMs from the UF support, the PEM-coated support was immersed for 10 min in a pH 10 buffer solution containing 0.060 M Na₂CO₃ and 0.596 M NaHCO₃. To evaluate the influence of colloidal deposition on the efficiency of PEM regeneration, both as-prepared and fouled PEM membranes were immersed in the buffer solution. For regeneration with backflushing, fouled mem-

branes were subjected to a three-step regeneration procedure:

- (i) Membranes were placed upside down in the membrane cell and backflushed with water for 1 h at an applied pressure differential that was 30 psi higher than that used in the preceding fouling experiments.
- (ii) Membranes were then soaked in the buffer solution and rinsed with water.
- (iii) Finally, a new PEM was applied to the surface of the cleaned membrane using the same layer-by-layer procedure as before.
- (iv) The hydraulic resistance and MgSO₄ rejection were measured after each step of the regeneration procedure.

4. Results and discussion

4.1. Charge, hydrophilicity, and water permeability of PEM membranes

Table 3 summarizes properties of the five PEM membranes and the commercial nanofiltration membrane (NF270) employed in this study. Both, the hydrophilicity and the surface charge of PEM membranes were primarily determined by the choice of the terminating polyelectrolyte and the ionic strength of the polyelectrolyte deposition solution (Table 1). As expected, terminating the polyelectrolyte film with a polycation (PAH or PDADMAC) produced a PEM with a positive surface charge, while terminating with a polyanion (PSS or PAA) resulted in a negative surface charge. To maximize the magnitude of the surface charge of the PEMs, the terminating layer was deposited from a solution with a high ionic strength (2.5 mol/L).

Additionally, Table 3 shows variations in the water contact angle among both positively and negatively charged PEM films (for SEM images see SD, Fig. S4). Notably, one PEM membrane, [PSS/PAH]₂ + [PAA/PAH]_{1.5}, was more hydrophilic and more negatively charged than the commercial NF270 membrane.

Varying the composition of PEMs also modifies the water permeabilities of these films. For example, PDADMAC-terminated coatings are known for their propensity to swell [37,56], so [PSS/PDADMAC]₄ films show the highest permeability to water (Table 3) of all PEMs studied. The number of deposited layers also affects flux as shown by a comparison of [PSS/PAH]₂ + [PAA/PAH]_{1.5} and [PSS/PAH]₂ + [PAA] films (Table 3).

4.2. Determining the salt permeability coefficient of PEM membranes

Expectedly, the *intrinsic* rejection, R_{in} , increased with an increase in the transmembrane pressure and the corresponding increase in the permeate flux (Fig. 2a), although the *observed* rejection, R_{obs} , decreased with an increase in the permeate flux for NF270 and all the PEM membranes (Fig. 2b). This indicates that higher R_{obs} can be achieved under lower concentration polarization condition by lowering permeate flux [37], or adding spacer onto the

Table 3

Surface and transport properties of the membranes in this study.

Membrane	Contact angle ^a , θ (°)	Streaming potential, ζ_m (mV)	Hydraulic resistance ^b , R_{m0} , $\times 10^{13}$ (m ⁻¹)
[PSS/PDADMAC] ₄	76 ± 6	21.4 ± 0.9	0.27 ± 0.09
[PSS/PAH] ₄	34 ± 3	13.4 ± 0.3	4.3 ± 0.7
[PSS/PAH] _{4.5}	36 ± 2	-10.8 ± 0.7	2.9 ± 0.4
[PSS/PAH] ₂ + [PAA]	27 ± 4	-0.9 ± 0.6	0.84 ± 0.32
[PSS/PAH] ₂ + [PAA/PAH] _{1.5}	20 ± 3	-7.7 ± 0.3	3.6 ± 1.1
NF 270	29 ± 3	-6.1 ± 0.5	2.5 ± 0.2

^a Contact angle for a water droplet on the membrane surface.^b The hydraulic resistance of the 50 kDa ultrafiltration membrane used as the support for PEM membranes was ca. $R_{m0} = 0.1 \times 10^{13} \text{ m}^{-1}$ after compaction.

membrane to create turbulent flow and thus reduce concentration polarization [57]. The increase trend of R_{in} is due to an increase in the amount of water, relative to the amount of salt, transported across the membrane at higher transmembrane pressures. When considering *observed* rejection, its decrease with an increase in the transmembrane pressure was due to the overcompensation of the better intrinsic rejection at higher permeate fluxes by the higher concentration polarization that led to a higher salt concentration gradient across the membrane and, consequently, higher salt flux.

The MgSO_4 permeability coefficient, P_s , of all membranes decreased with an increase in the MgSO_4 concentration near the membrane surface, C_m (Fig. 3).

This decrease in P_s somewhat mitigated decreases in the observed rejection due to the concentration polarization. The concentration dependence of the MgSO_4 permeability coefficient for NF270 was reported earlier by Al-Zoubi et al. [51]; in this paper

P_s was reported to increase with increasing MgSO_4 concentration, which is opposite to what we observed in our experiments. In our work, $0.19 < \tau < 0.83$ for all membranes, including NF270, for which $\tau \approx 0.42$.

For all membranes, the values of R_{in} determined for successively higher transmembrane pressure differentials, ΔP , asymptotically converged to a value close to 1 (Fig. 2), indicating that the reflection coefficient, σ , was close to 1. Although the permeability of PEM membranes with respect to MgSO_4 was higher than that of the NF270 membrane (Fig. 3), PEM membranes were highly selective ($\sigma \approx 1$) so that nearly complete MgSO_4 rejection by the membranes could in principle be achieved at sufficiently high fluxes if concentration polarization could be minimized.

It should be noted that because the mass transfer coefficient, k , is in the exponent (Eq. (2)), the values of the permeability coefficient, P_s , computed based on Eqs. (2) and (13) are sensitive to errors in the estimation of k using the Sherwood correlation (Eq. (1)). At higher permeate fluxes the error would be larger. For example, at the transmembrane pressure of 200 psi, the error of 10% in the estimated value of k would result in errors of ca. 38% and 28% in P_s , for NF270 and [PSS/PAH]_{4.5} membranes, respectively.

4.3. Rejection and permeate flux in colloidal fouling experiments: overall comparative assessment of NF270 and PEM membranes

Fig. 4 summarizes values of specific permeate flux, MgSO_4 rejection, and concentration polarization factor for all membranes before and after they were fouled by SiO_2 colloids. Several general observations can be made regarding the flux and rejection performance of NF270 and PEM membranes:

1. Initially, NF270 membranes exhibited the highest rejection (Fig. 4b) because of the low MgSO_4 permeability of NF270 (Fig. 3) and the relatively low value of the initial permeate flux (ca. $100 \text{ L}/(\text{m}^2 \text{ h})$) set for all membranes (Fig. 2). As discussed

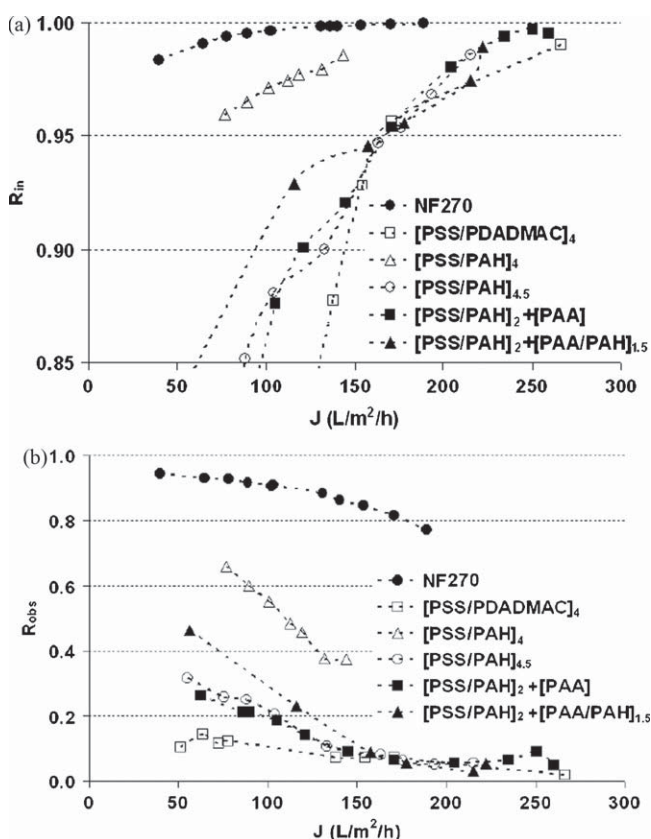


Fig. 2. Intrinsic (a) and observed (b) rejection of MgSO_4 by NF270 and PEM membranes as a function of permeate flux during filtration of colloid-free MgSO_4 electrolyte.

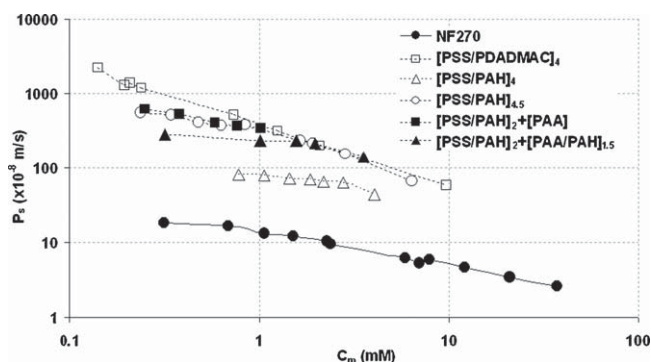


Fig. 3. Dependence of MgSO_4 permeability coefficient on MgSO_4 concentration at the membrane surface for NF270 and five PEM membranes.

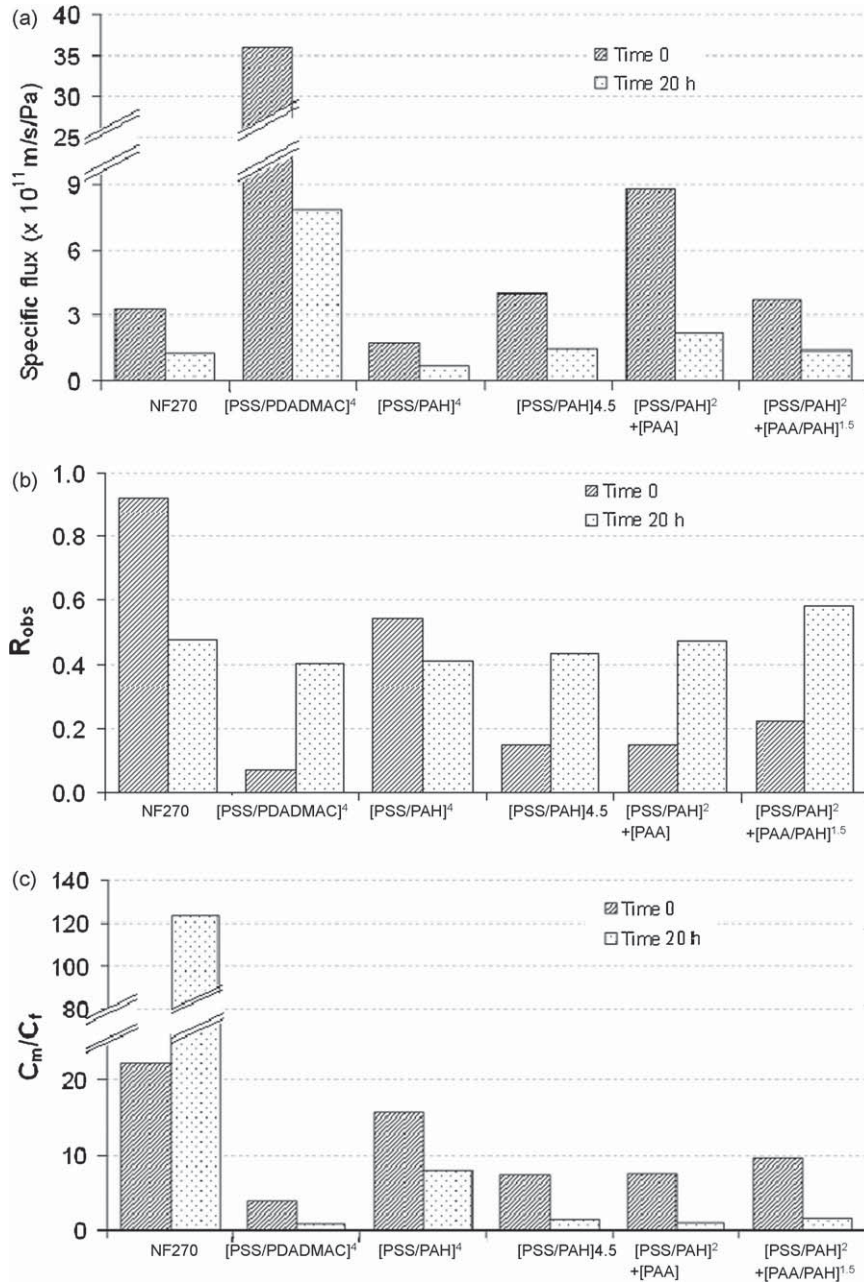


Fig. 4. Steady state values of the specific permeate flux (a), observed MgSO_4 rejection (b), and concentration polarization factor (c) for membranes before fouling (ca. $J = 2.8 \times 10^{-5}$ m/s, see Table 2) and after fouling with SiO_2 colloids.

above, at higher fluxes, the rejection of PEM membranes greatly increases.

- [PSS/PDADMAC]₄ stood out as a membrane with the highest specific permeate flux (Fig. 4a), which was due in part to the high hydraulic permeability of this membrane (Table 3) and in part due to its high permeability to MgSO_4 (Fig. 3) and the resulting low osmotic pressure.
- Colloidal fouling evened out the initial differences in rejection among the membranes.
- Remarkably, the observed salt rejection of all PEM membranes (except for [PSS/PAH]₄) fouled by colloids was higher than that of the same membrane before colloidal fouling occurred (Fig. 4b). This improvement in rejection was accompanied by a decrease in concentration polarization for those membranes (see Fig. 4c and the discussion in Section 4.4.2). With respect to NF270, the

combination of comparable rejection and superior specific permeate flux of [PSS/PDADMAC]₄ membrane clearly indicates that a membrane with highly beneficial properties is formed as a result of deposition of negatively charged colloids onto the surface of the [PSS/PDADMAC]₄ film.

Note that the initial rejection values are given for the initial permeate flux that varied only very slightly (27–31 $\mu\text{m/s}$) from one membrane to another (Table 2). The permeate flux after fouling (i.e. $t = 20$ h) was approximately the same (Fig. 5a ca. 40% of the initial permeate flux) for all membranes except for [PSS/PDADMAC]₄ and [PSS/PAH]₂ + [PAA]. For the latter two membranes, the flux after colloidal fouling was ca. 20% of the initial value. This has to be taken into account when comparing observed rejections of different membranes at 20 h.

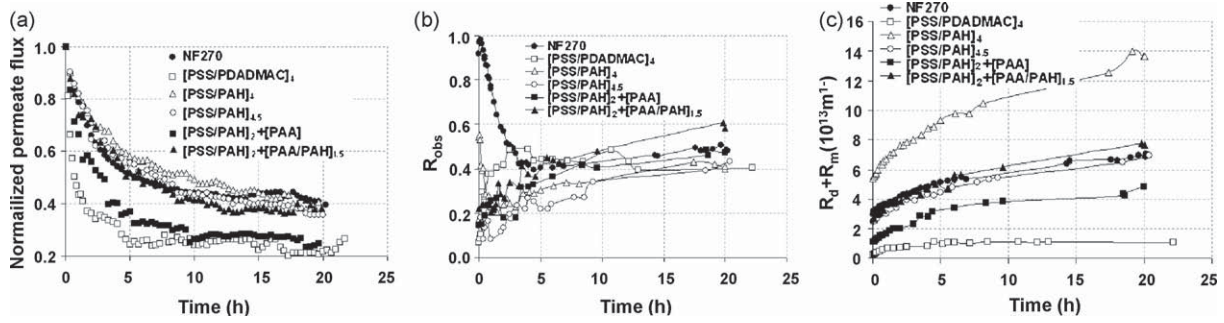


Fig. 5. Transient behavior of the normalized permeate flux (a), observed MgSO₄ rejection (b) and colloidal cake resistance (c) in experiments on the filtration of SiO₂ colloids.

4.4. Membrane performance in colloidal fouling experiments: transient behavior of permeate flux, MgSO₄ rejection, and cake resistance

Fig. 5 illustrates the transient behavior of normalized permeate flux, J , observed salt rejection, R_{obs} , and colloidal cake resistance, R_d , in colloidal fouling experiments. (The non-normalized values of the initial and final permeate flux are given in Fig. 4a.) Permeate flux and rejection data were recorded experimentally, while the R_d values were calculated after the contribution of the cake-enhanced osmotic pressure to the overall flux decline was accounted for (see Section 2.3).

There are two considerations that need to be taken into account when analyzing the data presented in Fig. 5.

- (i) Because higher rejections result in higher osmotic pressures, the temporal evolution of the permeate flux should be interpreted together with the rejection data. In turn, the observed rejection is a function of the salt concentration at the membrane surface, which depends on the amount of deposited colloids brought to the membrane. At the same time, the rate of colloidal deposition depends on the permeate flux. Thus, the dynamics of all three variables – J , R_{obs} , and R_d – are interdependent and should be analyzed together.
- (ii) Only at very early stages of the fouling experiments is the unfouled membrane surface exposed to the permeate flow. With the formation of a layer of colloidal particles on the membrane, the properties of the surface (charge and hydrophilicity) with which depositing colloids interact will be the properties of the already deposited colloids, not the as-prepared membranes.

The membranes fell into two categories: (i) membranes with anticipated MgSO₄ rejection behavior wherein the rejection decreased with the growth of the colloidal cake (NF270, [PSS/PAH]₄) and (ii) membranes with Mg rejection that increased with filtration time ([PSS/PDADMAC]₄, [PSS/PAH]_{4.5}, [PSS/PAH]₂ + PAA, and [PSS/PAH]₂ + PAA/PAH]_{1.5}).

4.4.1. Performance of NF270, [PSS/PAH]₄

For NF270 and [PSS/PAH]₄ membranes, MgSO₄ rejection decreased with filtration time as expected (Fig. 5b). This decrease in observed rejection was due to (i) the decrease in the permeate flux (Fig. 5a) and (ii) cake-enhanced concentration polarization (Fig. 6a). The concentration polarization factor, C_m/C_f , was calculated as described in Section 2.3. C_m/C_f for these two membranes increased significantly at first and then gradually declined to partially offset the initial increase (Fig. 6a); the corresponding trend in observed rejection (Fig. 5b) is consistent with the behavior reported earlier for LFC-1 [55] and BW30 [57] reverse osmosis membranes fouled by SiO₂ colloids. In experiments with SiO₂ colloids, the concentration polarization factor for NF270 was ca. 15 times higher

than that for the [PSS/PAH]₄ membranes after 20 h of colloidal filtration.

In experiments with SiO₂ colloids, the observed salt rejection of NF270 was significantly higher than that of [PSS/PAH]₄ during the initial stages of filtration (Fig. 5b), which explains the more than 15-fold higher polarization factor for NF270 during the early stages of the experiment (Fig. 6a, $t < 5$ h). During the filtration stage that followed, however, the rejection of all membranes was similar and yet the polarization factor of NF270 was still up to 15 times higher than that of [PSS/PAH]₄ membrane (Fig. 6; also see SD, Fig. S7). With the resistance of the cake formed on the membrane surface being higher for [PSS/PAH]₄ than for NF270 (Fig. 5c), the large difference in the polarization factor cannot be explained solely in terms of colloid and MgSO₄ transport. We hypothesize that the deposition of colloids alters the structure of the PEM film so that the extra resistance to the permeate flux due to the deposited colloids translates into a smaller increase in concentration polarization than for the

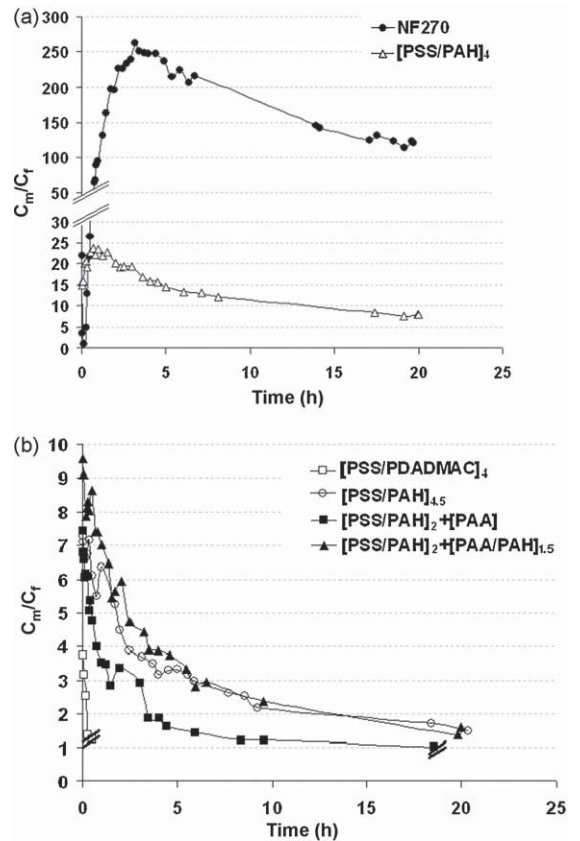


Fig. 6. Evolution of the concentration polarization factor during filtration of SiO₂ suspensions by different membranes.

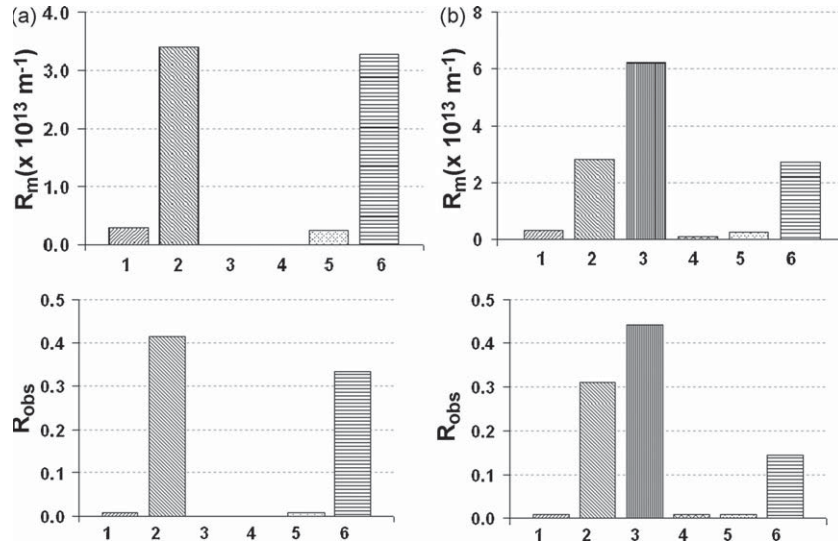


Fig. 7. Hydraulic resistance (R_m) and observed salt rejection (R_{obs}) values of a UF 50kDa support before (1) and after the following sequential steps (2) modification by a PEM; (3) filtration of SiO_2 for 20 h; (4) backflushing with water for 1 h; (5) soaking in pH 10 buffer for 10 min; (6) redeposition of a PEM layer. (In cases where no data are visible, those step(s) were omitted.) PEMs employed included (a) a $[\text{PSS}/\text{PAH}]_{4.5}$ film with no SiO_2 filtration; (b) a $[\text{PSS}/\text{PAH}]_{4.5}$ film with SiO_2 filtration and backflushing prior to soaking in pH 10 buffer.

more crosslinked commercial membranes such as NF270. It is possible that such changes in the membrane structure entail changes in the $P_s = P_s(C)$ dependence (Fig. 2), in which case the results on the concentration polarization factor (Figs. 4c and 6) and resistance of colloidal deposit (Fig. 5c) for PEM membranes would need to be interpreted with caution.

In evaluating flux and observed rejection data (Fig. 5a and b), one can see that, at steady state, the performance of the $[\text{PSS}/\text{PAH}]_4$ membrane under conditions of fouling by SiO_2 colloids is very similar to that of the NF270 membrane. Given the possible regeneration of PEM membranes, the $[\text{PSS}/\text{PAH}]_4$ films might provide an attractive alternate for controlling the fouling by negatively charged SiO_2 particles.

4.4.2. Performance of $[\text{PSS}/\text{PAH}]_2 + [\text{PAA}]$, $[\text{PSS}/\text{PAH}]_2 + [\text{PAA}/\text{PAH}]_{1.5}$, and $[\text{PSS}/\text{PDADMAC}]_4$, $[\text{PSS}/\text{PAH}]_{4.5}$ membranes

The second category of membranes consists of the positively charged $[\text{PSS}/\text{PDADMAC}]_4$, neutral $[\text{PSS}/\text{PAH}]_2 + [\text{PAA}]$, and negatively charged $[\text{PSS}/\text{PAH}]_{4.5}$ and $[\text{PSS}/\text{PAH}]_2 + [\text{PAA}]_{1.5}$ membranes. The rejections of these four PEM membranes unexpectedly increased with filtration time. Furthermore, for these membranes the calculated concentration polarization factor decreased with the filtration time. For $[\text{PSS}/\text{PDADMAC}]_4$ (and, at the very end of filtration, for $[\text{PSS}/\text{PAH}]_2 + [\text{PAA}]_{1.5}$) the concentration polarization factor, computed in the assumption of the constant $P_s(C_m)$ dependence, was found to decline over the time of filtration to below 1, which is the domain of unphysical values (Fig. 6b). We attributed this to the possible decrease of P_s with the deposition of significant amount of SiO_2 colloids onto the PEM surface or even inside the PEM film. For $[\text{PSS}/\text{PDADMAC}]_4$ membrane covered by only a submonolayer of SiO_2 colloids no significant changes in $P_s(C_m)$ were observed (see SD). Generally, for a net depositional system, such as a membrane filter prior to the attainment of the steady state flux, the trend of increasing rejection with time cannot be explained without invoking changes in the membrane properties. A modification of the salt-rejecting properties of these membranes due to changes in the PEM structure upon colloidal deposition is a likely explanation of such a trend. Thus, the above results bring into question the model's basic assumption that the membrane transport coefficients remain unchanged with time.

We hypothesize that a PEM-colloid nanocomposite was formed on the UF support surface. This hypothesis is based on the anomalous behavior of rejection and concentration polarization factor as well as on the observations that PEM films can swell. PDADMAC-capped $[\text{PSS}/\text{PDADMAC}]_4$ films in water have a swollen thickness of ca. 100 nm [56], which is comparable to the diameter of SiO_2 particles and could allow the particles to be embedded inside the PEMs. In this regard, it is interesting to note that during colloidal filtration $[\text{PSS}/\text{PDADMAC}]_4$ exhibited the most rapid flux decline among the six membranes, but the increase in cake resistance was not as rapid (see SD, Fig. S7) as it was for the other membranes resulting in the lowest steady state R_d value among all membranes. One possible reason for the improved rejection by such PEM-colloid nanocomposite films is that the colloids create a charged layer that contributes to rejection.

4.5. Regeneration of $[\text{PSS}/\text{PAH}]_4$ and $[\text{PSS}/\text{PAH}]_{4.5}$ films

Poly(allylamine hydrochloride) becomes weakly charged at high pH and thus dissociation of multilayers composed of $[\text{PSS}/\text{PAH}]$ (and, thereby, removal of the PEM from the UF support [56,58]) can be achieved by increasing the pH of the external solution [5,41,59]. PEMs can potentially then be re-deposited (i.e. regenerated at the support surface) from low pH solutions. The removal of (1) as-deposited and (2) colloid-fouled $[\text{PSS}/\text{PAH}]_4$ or $[\text{PSS}/\text{PAH}]_{4.5}$ PEM films from the UF support was monitored by recording changes in hydraulic resistance, $R_m = (\mu \cdot L_p)^{-1}$, and observed salt rejection, R_{obs} , of the membrane at different steps of the regeneration procedure (Fig. 7).

After soaking as-prepared PEM membranes (Fig. 7a; $[\text{PSS}/\text{PAH}]_{4.5}$ membrane) in the pH 10 buffer solution (step 5 in Fig. 7a), the values of R_m and R_{obs} both decreased to the level typical of the UF membrane (step 1 in Fig. 7a), suggesting removal of the polyelectrolyte film. (Note that the relatively low values of observed rejection by the PEM membranes are due to concentration polarization.) Reapplication of the PEM (step 6) returned R_m and R_{obs} to nearly the levels characteristic of an as-prepared PEM-coated membrane. The same procedure was followed with $[\text{PSS}/\text{PAH}]_{4.5}$ and $[\text{PSS}/\text{PAH}]_4$ membranes fouled by SiO_2 , it seems that the fouling did inhibit the regeneration of PEMs by the low

values of R_m and R_{obs} after step 6 (data not shown). Therefore, the simple soaking of the fouled membrane in the buffer solution apparently was not sufficient to completely remove PEMs and the foulants. SEM images taken for this membrane after step 6 (see SD; Fig. S4d) confirmed the presence of residual SiO_2 colloids on the membrane surface. The regeneration by soaking alone was not successful for $[\text{PSS}/\text{PAH}]_4$ and $[\text{PSS}/\text{PAH}]_{4.5}$ fouled by SiO_2 .

The backflushing step greatly improved the efficiency of PEM regeneration (Fig. 7b, step 6). The membranes were backflushed with ultrapure water (step 4 in Fig. 7b; $[\text{PSS}/\text{PAH}]_{4.5}$ membrane) to remove $[\text{PSS}/\text{PAH}]_{4.5}$ films from membranes severely fouled by SiO_2 colloids (300 mg(SiO_2)/L, 20 h filtration). After backflushing-assisted PEM removal and PEM regeneration, the value of R_m returned to the level characteristic of an as-prepared PEM membrane. The value of R_{obs} increased as well although only to about 50% of the rejecting capability of an as-prepared PEM membrane. While the composition of the soaking solution and backflushing duration need to be optimized to improve the efficiency of regeneration, the demonstrated feasibility of backflushing points to the possibility of using PEM films as regenerable nanofiltration coatings with controlled charge, hydrophilicity, and permeability.

5. Conclusions

By choosing constituent polyelectrolytes and by adjusting conditions of their deposition, supported PEM membranes with controllable surface charge, hydrophilicity and permeability to water and salt were designed and characterized in terms of their ion transport properties and resistance to colloidal fouling. It was found that:

1. Highly hydrophilic and charged PEMs could be designed.
2. Reflection coefficient of PEM membranes were estimated to be close to 1 indicating that the designed PEM membranes were highly selective and could achieve nearly complete intrinsic rejection of MgSO_4 at sufficiently high fluxes.
3. Salt permeability coefficients of NF270 and all PEM membranes exhibited power law dependence on concentration: $P_s \propto C^{-\tau}$, $0.19 < \tau < 0.83$.
4. Under the highly fouling conditions employed in this study, certain PEMs ($[\text{PSS}/\text{PAH}]_4$) had steady-state performance similar to that of the commercial NF270 membranes, especially in the longer term (>5 h).
5. The separation properties of certain PEMs improved dramatically with the deposition of colloids onto their surface. For these membranes, the concentration polarization decreased and MgSO_4 rejection increased with an increase in the amount of deposited colloids. We hypothesize that a PEM-colloid nanocomposite was formed on the UF support surface as a result of colloidal fouling of the PEM film.
6. The feasibility of regenerating the PEM coating has been demonstrated. Although regeneration of highly fouled membranes by soaking alone was inhibited by the incomplete removal of deposited colloids, an additional backflushing step resulted in an almost complete removal of the fouled PEMs and enabled reassembly of a PEM film with permeabilities similar to those of the initial PEM membrane and 50% lower rejection.

In summary, PEM membranes showed high selectivity and could be regenerated under appropriate conditions. Such membranes can potentially be designed to combine desirable ion separation characteristics, anti-adhesive surface properties and regenerability of the separation layer.

Acknowledgements

This material is based upon work supported by the National Science Foundation under grant no. OISE-0530174. We also thank Dow-FilmTec and Pall Corporation for providing us with membrane samples and Nissan Chemical America Corporation for supplying the silica suspension.

Appendix A. Supplementary data

Supplementary data associated with this article can be found, in the online version, at doi:10.1016/j.memsci.2009.11.059.

Nomenclature

A	membrane filtration area (m^2)
C_f	solute concentration in the bulk of the feed solution (mol/L)
C_m	solute concentration at the membrane surface (mol/L)
C_p	solute concentration in the permeate (mol/L)
D	diffusion coefficient of the solute (m^2/s)
d_h	hydraulic diameter of the membrane channel (m)
I_c	ionic strength (mol/L)
J	permeate volume flux across the membrane (m/s)
J_s	solute flux across the membrane (m/s)
k	mass transfer coefficient (m/s)
L	length of the membrane channel (m)
ΔL	colloidal cake thickness (m)
L_p	hydraulic permeability ($\text{m}/(\text{s Pa})$)
n	total number of constituent ions in the salt
ΔP	transmembrane pressure differential (Pa)
\bar{P}	local solute permeability coefficient (m^2/s)
P_s	solute permeability coefficient (m/s)
R_{obs}	observed rejection of the solute
R_{in}	intrinsic rejection of the solute
R_d	resistance of the deposited colloidal layer (m^{-1})
R_{m0}	initial hydraulic resistance of the membrane to pure water (m^{-1})
R_m	hydraulic resistance of the membrane to pure water after membrane conditioning (m^{-1})
R	universal gas constant
t	time (s)
T	absolute temperature (K)
$\Delta\pi_m$	osmotic pressure across the membrane (Pa)
ζ_m	streaming potential (mV)
ζ_p	zeta potential (mV)
θ	contact angle ($^\circ$)
μ	dynamic viscosity of water ($\text{N s}/\text{m}^2$)
ρ	density of particle (kg/m^3)
σ	reflection coefficient
τ	ratio of the valency of coions to the valency of counterions in the approximation of excluded coions
ϕ	osmotic coefficient
ω	solute permeability

References

- [1] G. Decher, J.D. Hong, Buildup of ultrathin multilayer films by a self-assembly process: 2. Consecutive adsorption of anionic and cationic bipolar amphiphiles and polyelectrolytes on charged surfaces, Ber. Bunsen. Phys. Chem. 95 (1991) 1430–1434.
- [2] G. Decher, J.D. Hong, J. Schmitt, Buildup of ultrathin multilayer films by a self-assembly process: 3. Consecutively alternating adsorption of anionic and

- cationic polyelectrolytes on charged surfaces, *Thin Solid Films* 210 (1992) 831–835.
- [3] G. Decher, Fuzzy nanoassemblies: toward layered polymeric multicomposites, *Science* 277 (1997) 1232–1237.
 - [4] P. Bertrand, A. Jonas, A. Laschewsky, R. Legras, Ultrathin polymer coatings by complexation of polyelectrolytes at interfaces: suitable materials, structure and properties, *Macromol. Rapid Commun.* 21 (2000) 319–348.
 - [5] M. SchÖnhoff, Layered polyelectrolyte complexes: physics of formation and molecular properties, *J. Phys. Condens. Mater.* 15 (2003) 1781–1808.
 - [6] M. Müller, J. Meier-Haack, S. Schwarz, H.M. Buchhammer, E.J. Eichhorn, A. Janke, B. Kessler, J. Nagel, M. Oelmann, T. Reihs, K. Lunkwitz, Polyelectrolyte multilayers and their interactions, *J. Adhesion* 80 (2004) 521–547.
 - [7] M. Müller, T. Rieser, K. Lunkwitz, J. Meier-Haack, Polyelectrolyte complex layers: a promising concept for antifouling coatings verified by in-situ ATR-FTIR spectroscopy, *Macromol. Rapid Commun.* 20 (1999) 607–611.
 - [8] J. Meier-Haack, T. Rieser, W. Lenk, D. Lehmann, S. Berwald, S. Schwarz, Effect of polyelectrolyte complex layers on the separation properties and the fouling behavior of surface and bulk modified membranes, *Chem. Eng. Technol.* 23 (2000) 114–118.
 - [9] T. Rieser, K. Lunkwitz, S. Berwald, J. Meier-Haack, M. Müller, F. Cassel, Z. Dioszeghy, F. Simon, Surface modification of microporous polypropylene membranes by polyelectrolyte multilayers, in membrane formation and modification, *ACS Sym. Ser.* (2000) 189–204.
 - [10] M. Müller, T. Rieser, P.L. Dubin, K. Lunkwitz, Selective interaction between proteins and the outermost surface of polyelectrolyte multilayers: influence of the polyanion type, pH and salt, *Macromol. Rapid Commun.* 22 (2001) 390–395.
 - [11] J. Meier-Haack, M. Müller, Use of polyelectrolyte multilayer systems for membrane modification, *Macromol. Sym.* 188 (2002) 91–103.
 - [12] J.D. Mendelsohn, S.Y. Yang, J. Hiller, A.I. Hochbaum, M.F. Rubner, Rational design of cytophilic and cytophobic polyelectrolyte multilayer thin films, *Biomacromolecules* 4 (2003) 96–106.
 - [13] S.Y. Yang, J.D. Mendelsohn, M.F. Rubner, New class of ultrathin, highly cell-adhesion-resistant polyelectrolyte multilayers with micropatterning capabilities, *Biomacromolecules* 4 (2003) 987–994.
 - [14] F. Boulmedais, B. Frisch, O. Etienne, P. Lavalle, C. Picart, J. Ogier, J.C. Voegel, P. Schaaf, C. Egles, Polyelectrolyte multilayer films with pegylated polypeptides as a new type of anti-microbial protection for biomaterials, *Biomaterials* 25 (2004) 2003–2011.
 - [15] D.S. Salloum, J.B. Schlenoff, Protein adsorption modalities on polyelectrolyte multilayers, *Biomacromolecules* 5 (2004) 1089–1096.
 - [16] D.L. Elbert, C.B. Herbert, J.A. Hubbell, Thin polymer layers formed by polyelectrolyte multilayer techniques on biological surfaces, *Langmuir* 15 (1999) 5355–5362.
 - [17] L. Richert, P. Lavalle, E. Payan, X.Z. Shu, G.D. Prestwich, J.F. Stoltz, P. Schaaf, J.C. Voegel, C. Picart, Layer by layer buildup of polysaccharide films: physical chemistry and cellular adhesion aspects, *Langmuir* 20 (2004) 448–458.
 - [18] M.T. Thompson, M.C. Berg, I.S. Tobias, M.F. Rubner, K.J. Van Vliet, Tuning compliance of nanoscale polyelectrolyte multilayers to modulate cell adhesion, *Biomaterials* 26 (2005) 6836–6845.
 - [19] A. Schneider, G. Francius, R. Obeid, P. Schwinte, J. Hemmerle, B. Frisch, P. Schaaf, J.C. Voegel, B. Senger, C. Picart, Polyelectrolyte multilayers with a tunable Young's modulus: influence of film stiffness on cell adhesion, *Langmuir* 22 (2006) 1193–1200.
 - [20] Y.X. Lu, J.Q. Sun, J.C. Shen, Cell adhesion properties of patterned poly(acrylic acid)/poly(allylamine hydrochloride) multilayer films created by room-temperature imprinting technique, *Langmuir* 24 (2008) 8050–8055.
 - [21] J.H. Fu, J. Ji, W.Y. Yuan, J.C. Shen, Construction of anti-adhesive and antibacterial multilayer films via layer-by-layer assembly of heparin and chitosan, *Biomaterials* 26 (2005) 6684–6692.
 - [22] J.A. Lichter, M.T. Thompson, M. Delgadillo, T. Nishikawa, M.F. Rubner, K.J. Van Vliet, Substrata mechanical stiffness can regulate adhesion of viable bacteria, *Biomacromolecules* 9 (2008) 1571–1578.
 - [23] R. von Klitzing, B. Tieke, Polyelectrolyte membranes, in: *Polyelectrolytes with Defined Molecular Architecture I*, Springer-Verlag Berlin, Berlin, 2004, pp. 177–210.
 - [24] J.J. Harris, J.L. Stair, M.L. Bruening, Layered polyelectrolyte films as selective, ultrathin barriers for anion transport, *Chem. Mater.* 12 (2000) 1941–1946.
 - [25] L. Krasemann, B. Tieke, Selective ion transport across self-assembled alternating multilayers of cationic and anionic polyelectrolytes, *Langmuir* 16 (2000) 287–290.
 - [26] B.W. Stanton, J.J. Harris, M.D. Miller, M.L. Bruening, Ultrathin, multilayered polyelectrolyte films as nanofiltration membranes, *Langmuir* 19 (2003) 7038–7042.
 - [27] R. Malaisamy, M.L. Bruening, High-flux nanofiltration membranes prepared by adsorption of multilayer polyelectrolyte membranes on polymeric supports, *Langmuir* 21 (2005) 10587–10592.
 - [28] A. El-Hashani, A. Toutianoush, B. Tieke, Layer-by-layer assembled membranes of protonated 18-azacrown-6 and polyvinylsulfate and their application for highly efficient anion separation, *J. Phys. Chem. B* 111 (2007) 8582–8588.
 - [29] A.M. Hollman, D. Bhattacharyya, Pore assembled multilayers of charged polypeptides in microporous membranes for ion separation, *Langmuir* 20 (2004) 5418–5424.
 - [30] W. Jin, A. Toutianoush, B. Tieke, Use of polyelectrolyte layer-by-layer assemblies as nanofiltration and reverse osmosis membranes, *Langmuir* 19 (2003) 2550–2553.
 - [31] L. Krasemann, B. Tieke, Composite membranes with ultrathin separation layer prepared by self-assembly of polyelectrolytes, *Mater. Sci. Eng. C: Biomimetic Supramol. Syst.* 8–9 (1999) 513–518.
 - [32] A. Toutianoush, B. Tieke, Selective transport and incorporation of highly charged metal and metal complex ions in self-assembled polyelectrolyte multilayer membranes, *Mater. Sci. Eng. C: Biomimetic Supramol. Syst.* 22 (2002) 135–139.
 - [33] X. Liu, M.L. Bruening, Size-selective transport of uncharged solutes through multilayer polyelectrolyte membranes, *Chem. Mater.* 16 (2004) 351–357.
 - [34] M.D. Miller, M.L. Bruening, Controlling the nanofiltration properties of multilayer polyelectrolyte membranes through variation of film composition, *Langmuir* 20 (2004) 11545–11551.
 - [35] W. Jin, A. Toutianoush, B. Tieke, Size- and charge-selective transport of aromatic compounds across polyelectrolyte multilayer membranes, *Appl. Surf. Sci.* 246 (2005) 444–450.
 - [36] S.U. Hong, M.L. Bruening, Separation of amino acid mixtures using multilayer polyelectrolyte nanofiltration membranes, *J. Membr. Sci.* 280 (2006) 1–5.
 - [37] L. Ouyang, R. Malaisamy, M.L. Bruening, Multilayer polyelectrolyte films as nanofiltration membranes for separating monovalent and divalent cations, *J. Membr. Sci.* 310 (2008) 76–84.
 - [38] S.U. Hong, R. Malaisamy, M.L. Bruening, Separation of fluoride from other monovalent anions using multilayer polyelectrolyte nanofiltration membranes, *Langmuir* 23 (2007) 1716–1722.
 - [39] D. Yoo, S.S. Shiratori, M.F. Rubner, Controlling bilayer composition and surface wettability of sequentially adsorbed multilayers of weak polyelectrolytes, *Macromolecules* 31 (1998) 4309–4318.
 - [40] S.T. Dubas, J.B. Schlenoff, Factors controlling the growth of polyelectrolyte multilayers, *Macromolecules* 32 (1999) 8153–8160.
 - [41] S.T. Dubas, J.B. Schlenoff, Polyelectrolyte multilayers containing a weak polyacid: construction and deconstruction, *Macromolecules* 34 (2001) 3736–3740.
 - [42] R. Rautenbach, R. Albrecht, *Membrane processes.*, John Wiley & Sons Ltd., New York, 1989.
 - [43] J.S. Newman, *Electrochemical Systems*, 2nd ed., Prentice Hall, USA, 1991.
 - [44] A.S. Michaels, New separation technique for CPI, *Chem. Eng. Prog.* 64 (1968) 31–43.
 - [45] O. Kedem, A. Katchalsky, Thermodynamic analysis of the permeability of biological membranes to non-electrolytes, *Biochim. Biophys. Acta* 27 (1958) 229–246.
 - [46] K.S. Pitzer, Thermodynamics of electrolytes. 1. Theoretical basis and general equations, *J. Phys. Chem.-US* 77 (1973) 268–277.
 - [47] R.C. Phutela, K.S. Pitzer, Heat-capacity and other thermodynamic properties of aqueous magnesium-sulfate to 473-K, *J. Phys. Chem.* 90 (1986) 895–901.
 - [48] K.S. Spiegler, O. Kedem, Thermodynamics of hyperfiltration (reverse osmosis): criteria for efficient membranes, *Desalination* 1 (1966) 311–326.
 - [49] X.L. Wang, T. Tsuru, M. Togoh, S. Nakao, S. Kimura, Evaluation of pore structure and electrical-properties of nanofiltration membranes, *J. Chem. Eng. Jpn.* 28 (1995) 186–192.
 - [50] A.E. Yaroshchuk, Rejection of single salts versus transmembrane volume flow in RO/NF: thermodynamic properties, model of constant coefficients, and its modification, *J. Membr. Sci.* 198 (2002) 285–297.
 - [51] H. Al-Zoubi, N. Hilal, N.A. Darwish, A.W. Mohammad, Rejection and modelling of sulphate and potassium salts by nanofiltration membranes: neural network and Spiegler-Kedem model, *Desalination* 206 (2007) 42–60.
 - [52] O. Kedem, V. Freger, Determination of concentration-dependent transport coefficients in nanofiltration: defining an optimal set of coefficients, *J. Membr. Sci.* 310 (2008) 586–593.
 - [53] E.M.V. Hoek, A.S. Kim, M. Elimelech, Influence of crossflow membrane filter geometry and shear rate on colloidal fouling in reverse osmosis and nanofiltration separations, *Environ. Eng. Sci.* 19 (2002) 357–372.
 - [54] E.M.V. Hoek, M. Elimelech, Cake-enhanced concentration polarization: a new fouling mechanism for salt-rejecting membranes, *Environ. Sci. Technol.* 37 (2003) 5581–5588.
 - [55] H.Y. Ng, M. Elimelech, Influence of colloidal fouling on rejection of trace organic contaminants by reverse osmosis, *J. Membr. Sci.* 244 (2003) 215–226.
 - [56] M.D. Miller, M.L. Bruening, Correlation of the swelling and permeability of polyelectrolyte multilayer films, *Chem. Mater.* 17 (2005) 5375–5381.
 - [57] F. Wang, V.V. Tarabara, Coupled effects of colloidal deposition and salt concentration polarization on reverse osmosis membrane performance, *J. Membr. Sci.* 293 (2007) 111–123.
 - [58] J.J. Harris, M.L. Bruening, Electrochemical and in situ ellipsometric investigation of the permeability and stability of layered polyelectrolyte films, *Langmuir* 16 (2000) 2006–2013.
 - [59] H.H. Rmaile, J.B. Schlenoff, Internal pK(a)'s in polyelectrolyte multilayers: coupling protons and salts, *Langmuir* 18 (2002) 8263–8265.